ISSN 1027-4510, Journal of Surface Investigation. X-ray, Synchrotron and Neutron Techniques, 2016, Vol. 10, No. 1, pp. 177–186. © Pleiades Publishing, Ltd., 2016.
Original Russian Text © A.D. Yapryntsev, N.N. Gubanova, G.P. Kopitsa, A.Ye. Baranchikov, S.V. Kuznetsov, P.P. Fedorov, V.K. Ivanov, K.V. Ezdakova, V. Pipich, 2016, published in Poverkhnost'. Rentgenovskie, Sinkhrotronnye i Neitronnye Issledovaniya, 2016, No. 2, pp. 24–34.

Mesostructure of Yttrium and Aluminum Basic Salts Coprecipitated from Aqueous Solutions under Ultrasonic Treatment

A. D. Yapryntsev[a, d], N. N. Gubanova[b, c], G. P. Kopitsa[b, c], A. Ye. Baranchikov[d], S. V. Kuznetsov[e], P. P. Fedorov[e], V. K. Ivanov[d, f], K. V. Ezdakova[b], and V. Pipich[g]

[a] *Moscow State University, Moscow, 119991 Russia*

[b] *Konstantinov Petersburg Nuclear Physics Institute, National Research Centre "Kurchatov Institute", Gatchina, Leningrad oblast, 188300 Russia*

[c] *Institute of Silicate Chemistry, Russian Academy of Sciences, St. Petersburg, 199034 Russia*

[d] *Kurnakov Institute of General and Inorganic Chemistry, Russian Academy of Sciences, Moscow, 119991 Russia*

[e] *Prokhorov General Physics Institute, Russian Academy of Sciences, Moscow, 119991 Russia*

[f] *National Research Tomsk State University, Tomsk, 634050 Russia*

[g] *JCNS, Forschungszentrum Juelich GmbH, Outstation at MLZ, Garching, 85747 Germany*

e-mail: a.baranchikov@yandex.ru

Received July 1, 2015

Abstract—The influence of ultrasonic treatment on the micro- and mesostructures and fractal characteristics of amorphous powders of yttrium and aluminum basic salts (precursors for the synthesis of neodymium-activated yttrium–aluminum garnet, Nd:YAG, which were coprecipitated from aqueous solutions by different precipitants, namely, aqueous solutions of ammonia and ammonium bicarbonate) is studied. It is established that ultrasonication applied during the precipitation of the aforementioned powders does not significantly change the structure of the obtained materials but always leads to the formation of structures with a less homogeneous nuclear density, i.e., a more developed surface area. Moreover, the ultrasound-assisted precipitation of the hydroxocompounds by ammonium hydrocarbonate results in a certain increase in the surface fractal dimension and the degree of aggregation for mass-fractal aggregates of particles.

Keywords: ultrasonic treatment, ultrasmall-angle neutron scattering, fractal dimension, mesostructure, yttrium-aluminum garnet

DOI: 10.1134/S1027451016010365

INTRODUCTION

Lanthanide- or transition metal-doped yttrium–aluminum garnet ($Y_3Al_5O_{12}$), hereinafter referred to as YAG, is the most widespread material for fabricating the active elements of near- and mid-infrared (IR) solid-state lasers operating in the continuous and pulsed modes. YAG single crystals possess high mechanical strength, good chemical stability, and excellent thermal and optical characteristics. However, during the development of solid-state laser systems, engineers met with the fact that an enhancement in their efficiency and power is restricted by the properties of the single-crystal matrix. First of all, the foregoing refers to neodymium-doped yttrium–aluminum garnet (Nd:YAG). Despite considerable improvements in the growth technology, YAG single crystals have a number of drawbacks associated with doping (e.g., the zonality of crystal boules and others), which give rise to inhomogeneity of the optical characteristics, being especially high for large optical elements.

In recent years, one of the most significant achievements was the creation of laser ceramics [1–3], including YAG-based materials, the spectral-lasing characteristics of which are not inferior to those of single crystals, but exceed some of their parameters [1, 4–7]. Technological schemes underlying the obtainment of transparent ceramics involve several successive stages: powder-material synthesis, compaction, and compression (sintering and pressing). The most important stage of the preparation thereof is the fabrication of powders with characteristics that satisfy a number of requirements, such as, relatively small particle sizes (down to several hundreds of nanometers), a narrow particle size distribution, the absence of hard agglomerates, homogeneity of chemical-composition, and low content of impurities. At the same time, the solid-phase synthesis of YAG requires the use of high temperatures and a long treatment time [8–10].

YAG nanopowders are of independent interest because in them an increase in the yield of luminescence is observed upon the transition to the nanodisperse state in a number of cases. In the case of nano-

particles activated by lanthanide ions, such an effect is related to the following circumstances: the absence of low-energy phonons and a low phonon density leading to a cardinal change in the energy-transfer dynamics, variations in the local symmetry of cations in small clusters and on the surface of particles, and small Stark splitting due to a decrease in the crystal-field strength. To retain the useful size effect in products, either films or semitransparent 3D ceramics consisting of nanoscale grains are employed. It is pertinent to note that the characteristics of highly dispersed luminophores are determined mainly by the production method and the structure of the compounds formed during synthesis.

The aforementioned reasons have stimulated keen interest in the production of YAG powders, including those composed of nano- and submicroscale particles. There is now a large body of information on the features of the synthesis of similar materials based on soft chemistry approaches, e.g., deposition from aqueous solutions with the use of ammonia [11–13] and ammonium hydrocarbonate [14, 15] and sol–gel synthesis [16]. Hence, the issue about the structure of synthesized intermediate products remains almost completely unstudied.

Ultrasonic treatment is commonly used in the preparation of nanomaterials using soft-chemistry techniques. On account of the controlled application of specific physical phenomena arising when intense sound waves propagate through a liquid medium, it is possible to increase the rates of certain chemical reactions and obtain solid-phase products characterized by given chemical and phase compositions, micromorphologies, and porous structures. We note that ultrasonication was successfully employed to activate the processes taking place under hydrothermal conditions [17–20] and in solid-phase states [21–23]. At the same time, the character of ultrasonic influence on the processes by which metal hydroxocompounds are formed remains unknown in many respects.

The goal of this work is to analyze mesostructures of amorphous yttrium, aluminum, and neodymium hydroxocompounds coprecipitated from aqueous solutions under ultrasonic treatment with the help of ultrasmall-angle neutron scattering (USANS). The given materials are used as precursors for obtaining neodymium-activated YAG ceramics.

EXPERIMENTAL

Synthesis of the Samples

Coprecipitation by an ammonia solution. A mixture of aqueous solutions of $Al(NO_3)_3 \cdot 9H_2O$, $Y(NO_3)_3 \cdot 6H_2O$, and $Nd(NO_3)_3 \cdot 6H_2O$ (its cation molar ratio was 5 : 2.936 : 0.064), the total metal-ion concentration of which was 0.25 M, was slowly added to an aqueous ammonia solution (2.7 M) until pH 7.5 was attained. The pH of the medium was controlled using a Crison GLP-22 pH-meter equipped with a universal measuring probe and a thermal compensator. Precipitation was performed in a thermostated cell (its temperature was kept equal to 10 ± 1°C). Hydroxides were also deposited with the use of ultrasonic treatment under the same conditions. The ultrasonic-vibration source was a Bandelin Sonopuls HD 3200 generator with an immersion-type titanium waveguide. The ultrasonic-vibration frequency was 20 kHz at an effective acoustic-power density of 50 W/cm^2.

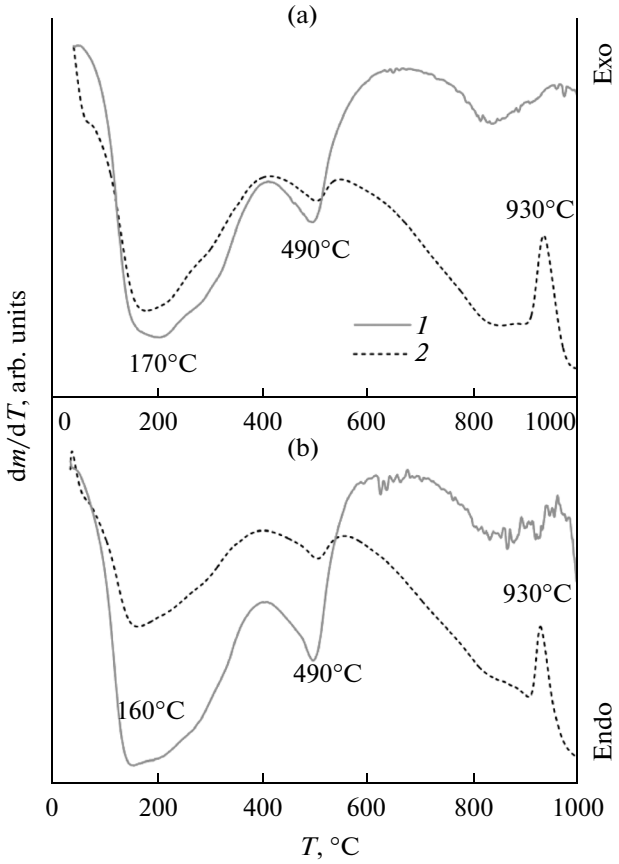

Fig. 1. Thermal analysis, namely, (*1*) DTG and (*2*) DTA, data obtained for the samples precipitated by aqueous ammonia (a) without and (b) with ultrasonic treatment.

After completion of the precipitation procedure, the prepared suspensions were intensely mixed for 15 min. The mixing of the suspensions deposited by ultrasonication was carried out in the ultrasonic field. Afterward, the precipitates were washed with distilled water for several times to reduce the conductivity of the parent solution to 0.5 mS, separated by centrifugation (10 000 rpm), and dried in air at a temperature of 50°C for 24 h.

The obtained powders were annealed in a furnace at 900°C for 5 h.

Coprecipitation by ammonium hydrocarbonate. A mixture of aqueous solutions of $Al(NO_3)_3 \cdot 9H_2O$, $Y(NO_3)_3 \cdot 6H_2O$, and $Nd(NO_3)_3 \cdot 6H_2O$ whose cation molar ratio was 5 : 2.936 : 0.064 and total metal-ion concentration was 0.25 M was added to an aqueous

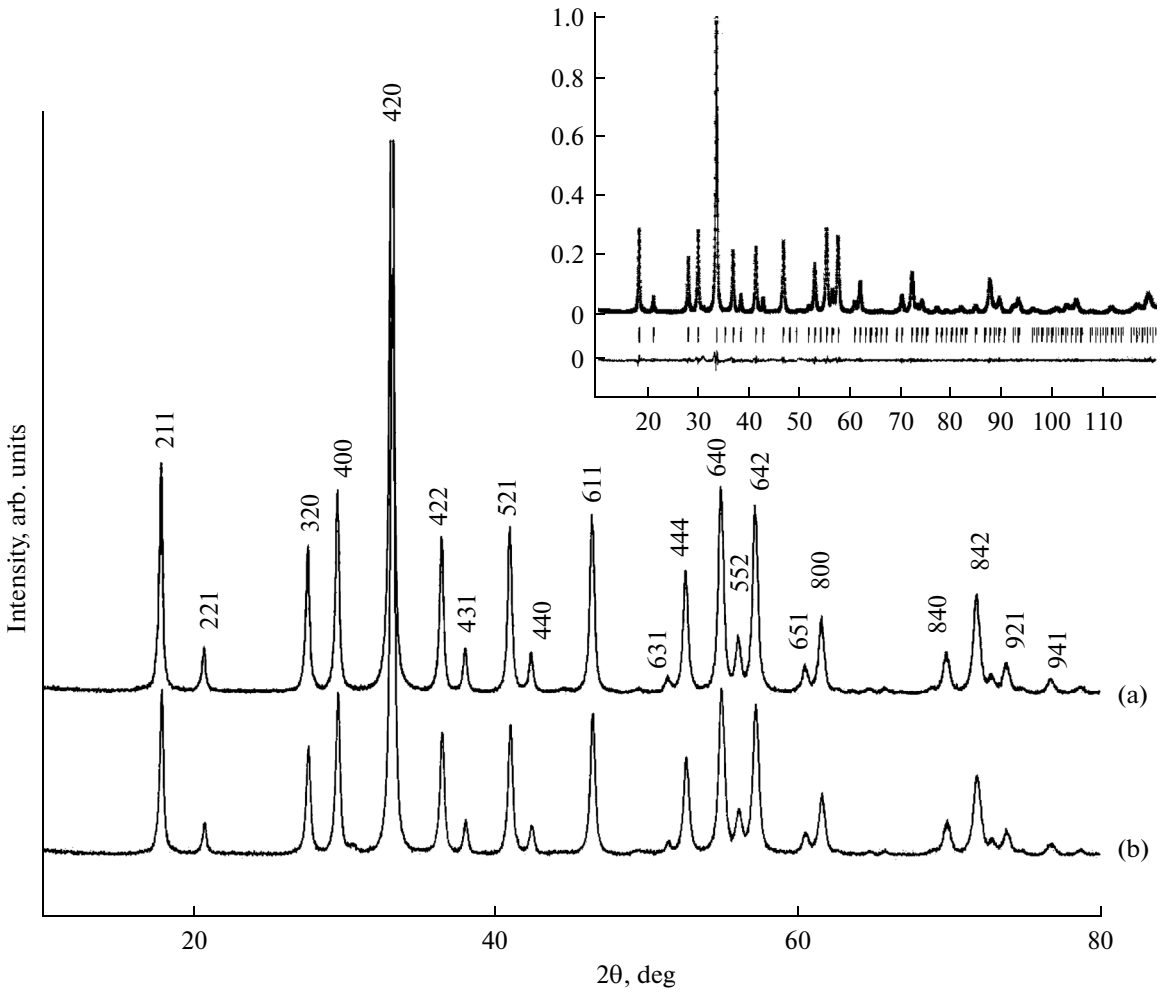

Fig. 2. X-ray diffraction patterns of the samples obtained by annealig of the YAG precursor precipitated by aqueous ammonia solutions (a) with and (b) without ultrasonic treatment. For reflections corresponding to the $Al_5Y_3O_{12}$ phase, Miller indices are designated according to PDF2, No. 33–40. In the case of the diffraction pattern (a), the results of the full-profile analysis are shown in the inset ($R_{wp} = 9.26$ and the goodness of fit is 2.58).

solution of NH_4HCO_3 (2 M). The process continued up to the attainment of pH 7.5. Deposition, drying, and annealing were performed under conditions similar to those used for the coprecipitation by ammonia.

Analysis of the Samples

Thermogravimetric analysis (TGA) and differential thermal analysis (DTA) of the samples was performed using a Perkin-Elmer Pyris Diamond analyzer at temperatures of 20–1000°C in air. The rate of heating was 10°C/min. X-ray diffraction (XRD) analysis of the samples was carried out using Rigaku D/MAX 2500 diffractometer (CuK_α radiation) at a goniometer rotation rate of 2°2θ/min. The diffraction maxima were identified using the JCPDS database.

USANS measurements were carried out using a KWS-3 high-resolution small-angle diffractometer (FRM-II reactor, Munich, Germany) operating with a toroidal focusing mirror, which allows a high resolution of the momentum transfer range (up to 1×10^{-4} Å^{-1}) to be attained [24, 25]. The spectra were measured at a neutron wavelength of $\lambda = 12.8$ Å ($\Delta\lambda/\lambda = 0.2$). The use of two sample–detector (S–D) distances (1 and 10 m) allowed neutron scattering intensities in the momentum transfer range $2.5 \times 10^{-4} < q < 1.4 \times 10^{-2}$ Å^{-1} to be measured. Scattered neutrons were recorded with the help of a 2D position-sensitive scintillation ^{6}Li detector.

During neutron measurements, the samples were placed between two quartz glasses pressed together. For each q range, the initial spectra were corrected using the standard procedure [26], taking into account scattering by the setup and quartz glasses, as well as the background. The obtained two-dimensional spectra were azimuthally averaged and converted to the absolute scale by normalization to the incoherent scattering cross section of plexiglass taking into account the detector sensitivity [26] and the thickness L_S of each sample. All measurements were conducted at room

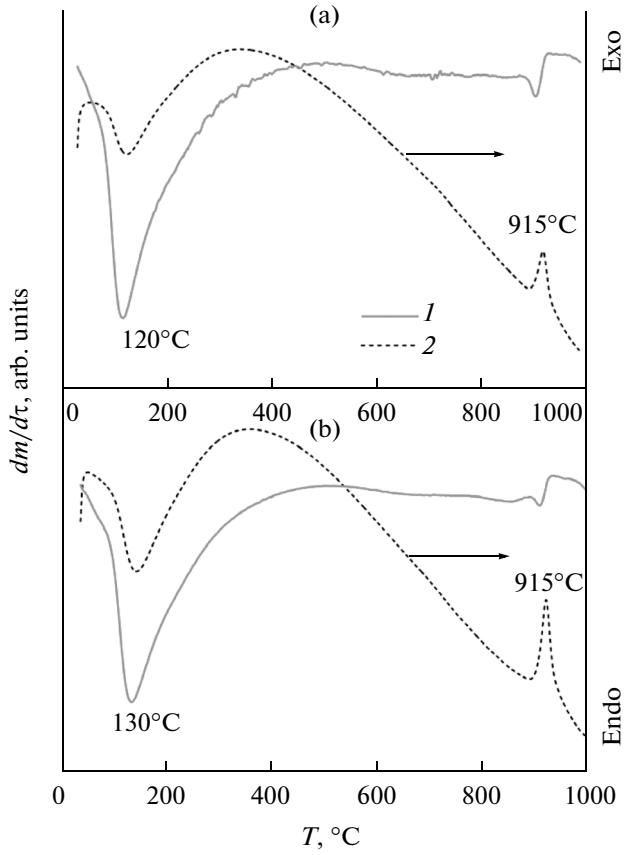

Fig. 3. Thermal analysis, namely, (*1*) DTG and (*2*) DTA, data obtained when the YAG precursor sample was precipitated by ammonium hydrocarbonate (a) without ultrasonic treatment and (b) under sonication.

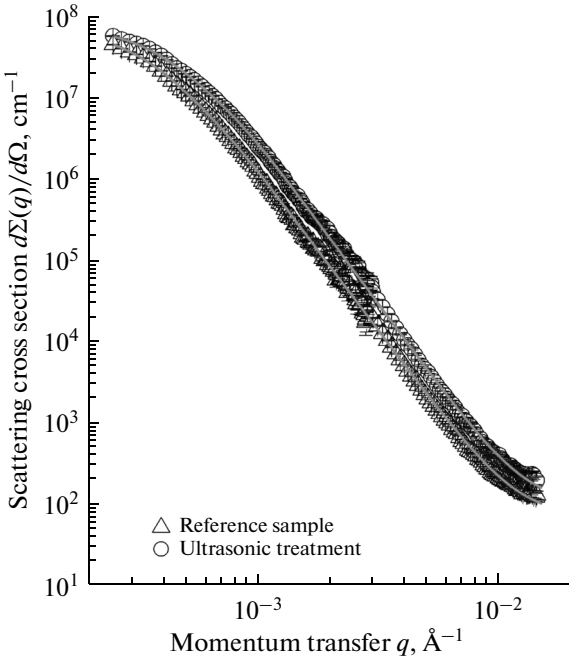

Fig. 4. USANS differential cross section $d\Sigma(q)/d\Omega$, for the samples precipitated by ammonia with and without ultrasonic treatment. Continuous curves correspond to experimental data fitted according to formula (4).

temperature. The preliminary data analysis was performed using the QtiKWS software package [27].

The USANS intensity $I_S(q)$ under consideration is defined as

$$I_S(q) = I(q) - TI_0(q), \quad (1)$$

where $I(q)$ is the q distribution of scattered neutrons after the sample, $I_0(q)$ is the corresponding distribution of the neutron beam without a sample, and T is the transmission coefficient of neutrons passed through the sample:

$$T = \frac{I(0)}{I_0(0)} = \exp\left(-\Sigma_{\text{tot}}L\right), \quad (2)$$

Here, $\Sigma_{\text{tot}} = \sigma_S + \sigma_a$ is the integrated cross section comprising nuclear scattering σ_S and absorption σ_a and L is the sample thickness.

The relationship between the measured USANS intensities and scattering law $S(q)$ is written as

$$I_S(q) = I_0 L \int F\left(q - q_1\right) S(q) dq_1, \quad (3)$$

where $F(q)$ is the resolution function of the setup approximated by a Gaussian function [28].

RESULTS AND DISCUSSION

Thermal Behavior of Yttrium and Aluminum Hydroxocompounds Precipitated by Ammonia

Figure 1a depicts the curves of differential thermogravimetry (DTG) and DTA for the sample precipitated by means of an ammonia solution without ultrasonication. It is likely that the broad endothermal peak with a minimum at 173°C corresponds to the removal of physically and chemically bound water. In the next stage of decomposition (with a maximum rate at 490°C) accompanied by the endothermal effect, a certain amount of chemically bound water and nitrates are removed. The latter were formed, e.g., due to interaction between the aqueous solutions of the bases and nitrates of rare-earth elements (REEs) (their supposed composition $REE_2(OH)_5(NO_3) \cdot 3H_2O$ [29–34]). For the given sample, the total mass loss (37%) turned out to be sufficiently close to the theoretical value (38%), which was calculated for an $Al(OH)_3 \cdot 0.3[(Y,Nd)_2(OH)_5(NO_3) \cdot 3H_2O]$ powder corresponding to the nominal content of metal cations in the initial solution.

The exothermal peak with a maximum observed at 930°C corresponds to YAG ($Y_{3-x}Nd_xAl_5O_{12}$) crystallization, which is confirmed by XRD data obtained upon 900°C annealing of the powders precipitated by ammonia (Fig. 2). In accordance with the Nd:YAG unit-cell parameters refined using the Jana2006 software package [35], $a = 12.0295(9)$ Å, i.e., is somewhat higher than the value inherent to YAG (12.0089 Å,

PDF2, No. 33–40). This implies that the neodymium(III) ion radius exceeds the yttrium(III) one if the coordination number is eight (1.109 and 1.019, respectively) [36].

When yttrium, aluminum, and neodymium hydroxocompounds are deposited by aqueous ammonia, ultrasonication hardly affects the thermal behavior of the corresponding powder (Fig. 1b) and the phase composition of the product of its annealing (Fig. 2). In the case of samples prepared with or without ultrasonic treatment, the total mass losses are identical, reaching 37–38%.

It should be emphasized that the influence of high-power ultrasonication on the composition and mesostructure of amorphous hydrated zirconium dioxide was previously studied. Ultrasound-assisted precipitation results in $ZrO_2 \cdot xH_2O$ gels with much lower content of absorbed nitrate species in comparison with ones precipitated without acoustic actions [37]. A similar effect is not observed in this work during the sonochemical synthesis of aluminum and neodymium hydroxocompounds. This is probably related to the fact that, in the given case, nitrate anions remain in a chemically bound, not absorbed, state. Therefore, in contrast to $ZrO_2 \cdot xH_2O$ gels, they are not adsorbed on the surfaces of metal-hydroxide particles.

Thermal Behavior of Yttrium and Aluminum Hydroxocompounds Precipitated by Ammonium Hydrocarbonate

Figures 3a and 3b present the DTG and DTA data obtained for samples that were precipitated by ammonium hydrocarbonate under normal conditions and with ultrasonic treatment, respectively. It can be seen that, in this case, differences in the thermal behavior of the corresponding powders are practically absent. On the whole, the presented data are analogous to those reported in [38, 39]. We note that the exothermal effect inherent to YAG crystallization from the precursors deposited by ammonium hydrocarbonate is shifted by 15° toward lower temperatures as compared to a similar effect typical of powders prepared by ammonia precipitation.

Thus, on the basis of all thermal analysis data discussed above, it can be concluded that ultrasonication has no notable influence on the chemical composition of yttrium, aluminum, and neodymium hydroxocompounds coprecipitated from aqueous solutions of metal salts by ammonia and ammonium hydrocarbonate.

Mesostructure of Yttrium and Aluminum Hydroxocompounds Precipitated by Ammonia Solutions

The USANS technique was employed to acquire information on mesostructure features of the aforementioned powders and reveal how ultrasonic treatment affects the aggregation of hydroxocompound particles during the precipitation process.

Figure 4 depicts the experimental dependences of the USANS differential macroscopic cross section, $d\Sigma(q)/d\Omega$, constructed on the double logarithmic scale. Data were determined for samples precipitated by ammonia with and without ultrasonic treatment. As can be seen, the scattering cross section of the sample prepared with ultrasonication is unambiguously higher than that of the reference sample, indicating that its nuclear-density homogeneity decreases at the mesoscopic scale (100–10000 Å) due to ultrasonic treatment. At the same time, a common property of both samples under study is that the corresponding curves involve three q ranges which greatly differ in terms of the behavior of the dependence of the small-angle scattering cross section $d\Sigma(q)/d\Omega$.

For example, at momentum transfer q of $7.5 \times 10^{-4} < q < 1 \times 10^{-2}$ Å^{-1}, the behavior of curve $d\Sigma(q)/d\Omega$ obeys the power law q^{-n}. The values of the exponent n were found from the slopes of straight-line segments in the experimental dependences $d\Sigma(q)/d\Omega$. Their values are 3.93 ± 0.02 (reference sample) and 4.00 ± 0.02 (sample synthesized with ultrasonication) (Table 1). This implies that the reference sample corresponds to scattering occurring at a fractal surface with the dimension $D_S = 6 - n = 2.07 \pm 0.02$. At the same time, for the sample formed with ultrasonication, $n = 4$ (Porod law) is undoubtable evidence that observed small-angle scattering at a neutron wavelength of $\lambda = 12.8$ Å occurs at inhomogeneities with practically smooth boundaries which is characteristic of the given experiment. In this case, $D_S = 2.00 \pm 0.02$.

In connection with this, the model of the two-phase porous structure (solid phase–pore medium) with the fractal surface of the phase interface is further employed to analyze the scattering at $q < 1 \times 10^{-2}$ Å^{-1} [40]. In accordance with this model, any object is composed of inhomogeneities (pores) with developed surfaces. Hence, when the total inhomogeneity (pore) surface area measured on the scale of its size R is proportional to R^2 and the surface measurement scale is $r \ll R$, the surface area turns out to be on the order of $R^2(R/r)^{\Delta}$, where $0 < \Delta < 1$ and $n = 4 - \Delta$. In this case, the surface fractal dimension ($D_S = 2 + \Delta$) will be greater than two.

For both samples, the behavior of the cross section $d\Sigma(q)/d\Omega$ deviates from the power law q^{-n} at small and large momentum transfer q irrespective of the conditions of synthesis. At low momentum transfer ($q < 7.5 \times 10^{-4}$ Å^{-1}), the given deviation is connected with the transition to the Guinier mode [41], where the scattering level is determined by the characteristic size R_c of independently scattering inhomogeneities. By analyzing the scattering process in the aforesaid mode, it is possible to estimate the gyration radius R_g of pores and, consequently, their characteristic size R_c. In the range of high momentum transfer, the cross section $d\Sigma(q)/d\Omega$ ceases to depend on q (i.e., becomes a constant) and is caused by incoherent scattering from

Table 1. Mesostructure parameters of yttrium, aluminum, and neodymium hydroxocompounds coprecipitated by ammonia (1) with and (2) without ultrasonic treatment. Their values were obtained by analyzing USANS data

Sample	T_S	Fitting parameter			
		$G \times 10^7$, cm^{-1}	R_g, Å	$B \times 10^{-6}$, cm^{-1} Å^{-n}	$D_S = 6 - n$
1	0.10 ± 0.01	8.16 ± 0.10	4460 ± 60	2.3 ± 0.1	2.00 ± 0.02
2	0.14 ± 0.01	7.66 ± 0.13	5320 ± 50	1.7 ± 0.1	2.07 ± 0.02

hydrogen atoms, which are included in the composition of the given samples as chemically bound water, and scattering at inhomogeneities whose sizes are on the order of the neutron wavelength λ used in the given experiment.

From the above, the unified exponential expression suggested for single-level structures [42] was employed to define scattering from the samples in the entire range under investigation:

$$\frac{d\Sigma(q)}{d\Omega} = G\exp\left(-\frac{q^2R_g^2}{3}\right) + \frac{B}{\hat{q}^n} + I_{\text{inc}}, \qquad (4)$$

where $\hat{q} = q/[\text{erf}(qR_g/6^{1/2})]^3$ is the momentum transfer q normalized to error function erf(x). The given procedure enables us to correctly describe the behavior of the cross section $d\Sigma(q)/d\Omega$ in the "intermediate" interval between $qR_c < 1$ (Guinier approximation) and $qR_c \gg 1$ (asymptotics of q^{-n}), which incorporates contributions to scattering from both inhomogeneities of the characteristic scale R_c and their local structure [42]. Parameter I_{inc} is a certain q-independent constant determined by incoherent scattering at hydrogen atoms, and amplitudes G and B are the Guinier and exponent prefactors, respectively. The first of them is directly proportional to the product of the number of inhomogeneities in the scattering volume by the average density ρ of neutron-scattering amplitudes [41], and the second depends on the local-structure characteristics, in particular, the surface fractal dimension D_S of scattering inhomogeneities [40]:

$$B(D_S) = \pi\rho^2\rho_0\Gamma(5 - D_S)\sin[(D_S - 1)(\pi/2)]N_0, \qquad (5)$$

where Γ is the gamma function and ρ_0 is the solid-phase density. In the case of a substance containing different atoms, ρ is defined as

$$\rho = \sum_i b_i N_i \frac{\rho_0 N_A}{M}. \qquad (6)$$

Here, N_A is the Avogadro number, M is the molar mass, b_i is the scattering length of element i in a molecule, and N_i is the number of element atoms. Constant N_0 and the specific surface of the fractal are related according to the expression $S_0 = N_0 r^{2-D_S}$, where r^{2-D_S} is specified by the measurement scale. In the case of smooth surfaces, $D_S = 2$ and $N_0 = S_0$.

To obtain the final results, expression (4) was convoluted with the resolution function of the setup. The experimental dependences of the differential cross section $d\Sigma(q)/d\Omega$ were analyzed via the least squares method (LSM) in the entire range under study. The results of this analysis are illustrated by Fig. 4 and summarized in Table 1.

The ultrasound-induced changes in the powder structure was qualitatively analyzed by comparing the scattering cross sections of yttrium, aluminum, and neodymium hydroxocompound powders coprecipitated by ammonia in an ultrasonic field and without an ultrasonic field. The results of the given comparison (Fig. 5) are plotted in double logarithmic coordinates as the differences between the scattering cross sections for the corresponding samples:

$$\frac{d\Sigma_{\text{Dif}}(q)}{d\Omega} = \frac{d\Sigma_{\text{US}}(q)}{d\Omega} - \frac{d\Sigma_{\text{K}}(q)}{d\Omega}. \qquad (7)$$

It follows from the presented data that the difference-curve ordinate is positive in the entire investigated range of q. This indicates that the reference sample makes a smaller contribution to small-angle neutron scattering (SANS) and, consequently, its nuclear density is more homogenous at the mesoscopic scale than that of the sample synthesized with ultrasonic treatment. This outcome coincides with the behavior of the transmission coefficient T_S of a neutron beam passed through a sample (Table 1). As is known, this parameter is inversely proportional to the integral scattering cross section and its reduction also evidences that nuclear-density fluctuations enhance in the powder deposited upon ultrasonication.

From analysis of the obtained structural parameters (Table 1) whereby the apparent small-angle scattering behavior is directly revealed, it is obvious that, firstly, the surface of scattering inhomogeneities is smoothed during ultrasonic treatment and, secondly, an appreciable decrease in the gyration radius R_g of the scattering inhomogeneities is observed. It should be noted that the radii R_g estimated from the given analysis are substantially underestimated (by ~30%). As is seen from Table 1, the transmission coefficients T_S for both samples are much less than 0.5, clearly indicating

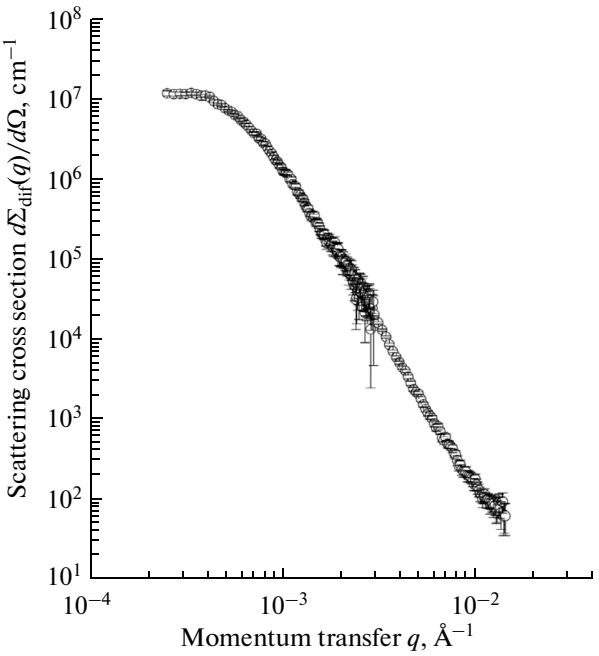

Fig. 5. Differences between the USANS cross sections for the powders precipitated by ammonia with and without ultrasonic treatment.

the existence of a considerable contribution from multiple scattering. It is known [43] that such a contribution distorts the observed small-angle scattering pattern just in the range of low momentum transfer, i.e., in the Guinier region. At the same time, the estimated surface fractal dimension D_S of the scattering inhomogeneities is correct because the contribution of multiple scattering to the scattering intensity distribution is negligibly small in the asymptotic limit q^{-n} [43].

Thus, when yttrium, aluminum, and neodymium hydroxocompounds are coprecipitated by mixing aqueous ammonia solutions and mixed solutions of metal salts, ultrasonication leads to two main effects. The first of them consists in some decrease in the nuclear-density homogeneity of the prepared powders and is analogous to that previously observed during the sonochemical synthesis of $ZrO_2 \cdot xH_2O$ [45]. The given decrease in the nuclear-density homogeneity can be attributed to the fact that aggregates with a greater porosity and higher specific surfaces are formed in the ultrasonic field. We note that the scattering cross section is directly proportional to the specific surface, as is defined by (4) and (5). The ultrasound-assisted generation of more porous aggregates is presumably related to shock-wave propagation and liquid microjets, which arise due to intense cavitation and increase in the frequency of collisions between colloidal particles in the suspension. The same physical phenomena induce a second effect of ultrasonic treatment: a ~20% decrease in the gyration radius R_g of large-scale aggregates.

Mesostructure of Yttrium and Aluminum Hydroxocompounds Precipitated by Ammonium Hydrocarbonate

Figure 6 presents the experimental dependences of the USANS differential cross section $d\Sigma(q)/d\Omega$ in the double logarithmic scale for the yttrium, aluminum, and neodymium hydroxocompounds powder samples precipitated by ammonium hydrocarbonate with and without ultrasonic treatment. As is clearly seen in Fig. 6, the observed scattering curves for the powders precipitated by ammonium hydrocarbonate differ substantially from those described above. This implies a noticeable discrepancy in the organization of the mesostructures of the samples precipitated by ammonia and ammonium hydrocarbonate. At the same time, it should be emphasized that, in the given case, the small-angle scattering cross section of the ultrasound-treated sample also exceeds that of the reference sample.

For both samples under study, the scattering process is characterized by the corresponding curves incorporating three ranges of momentum transfer, in which the behavior of the cross section $d\Sigma(q)/d\Omega$ satisfies the power law $q^{-\Delta}$ whose exponent Δ can take three values: $n1$, $n2$, and $n3$. The given pattern is typical of scattering at hierarchical three-level structures with different characteristic length scales and dissimilar aggregation types of each level.

Scattering from the first structural level manifests itself at large $q > 2 \times 10^{-3}$ Å^{-1} and is described by the power law q^{-n1} and restricted from above by the transition to the Guinier mode, where scattering is determined by the characteristic size R_{c1} of independently scattering particles (inhomogeneities) of the first structural level. The exponents $n1$ were found from the slopes of straight-line segments in experimental curves of the cross section $d\Sigma(q)/d\Omega$. Their values are 3.29 ± 0.03 (reference sample) and 3.18 ± 0.03 (ultrasound-treated sample) (Table 2). These estimates indicate that the first structural level of both samples is composed of particles (inhomogeneities) with a highly developed fractal surface of the phase interface. In this case, the surface fractal dimensions are $D_{S1} = 6 - n1 = 2.71 \pm 0.03$ and 2.82 ± 0.03, respectively.

Scattering from the second structural level is observed at momentum transfer q of $6 \times 10^{-4} < q < 2 \times 10^{-3}$ Å^{-1} and is defined by the power law q^{-n2}. The exponents $n2$ found from the slopes of straight-line segments in the experimental curves of $d\Sigma(q)/d\Omega$ are 1.53 ± 0.05 (reference sample) and 1.59 ± 0.04 (ultrasound-treated sample) (Table 2). As was noted above, this corresponds to scattering from objects (clusters) with a mass-fractal aggregation of inhomogeneities and the fractal dimensions $D_{m2} = n2 = 1.53 \pm 0.05$ and 1.59 ± 0.04, respectively. For the second structural level, the lower self-similarity boundary of mass-fractal clusters with an anisodiametrical branched structure depends on the characteristic size of the surface-fractal particles (inhomogeneities) of the first struc-

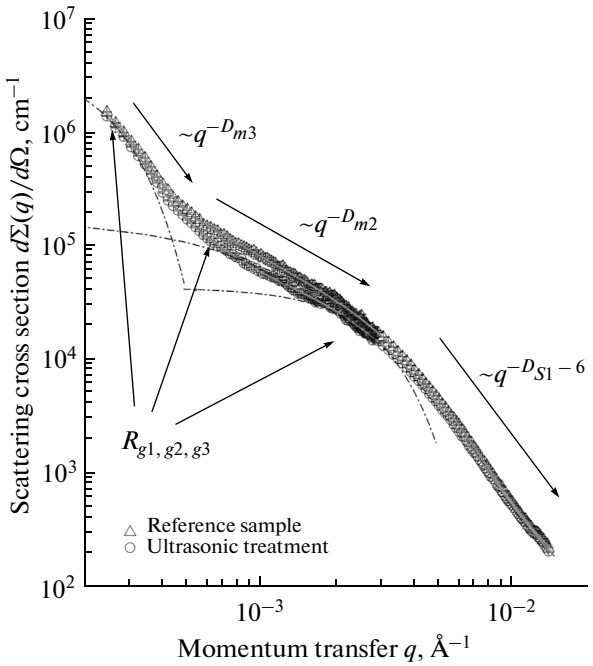

Fig. 6. USANS differential cross section, q, $d\Sigma(q)/d\Omega$, for the samples precipitated by ammonium hydrocarbonate without and with ultrasonic treatment. Continuous curves designate experimental data fitted according to formula (8).

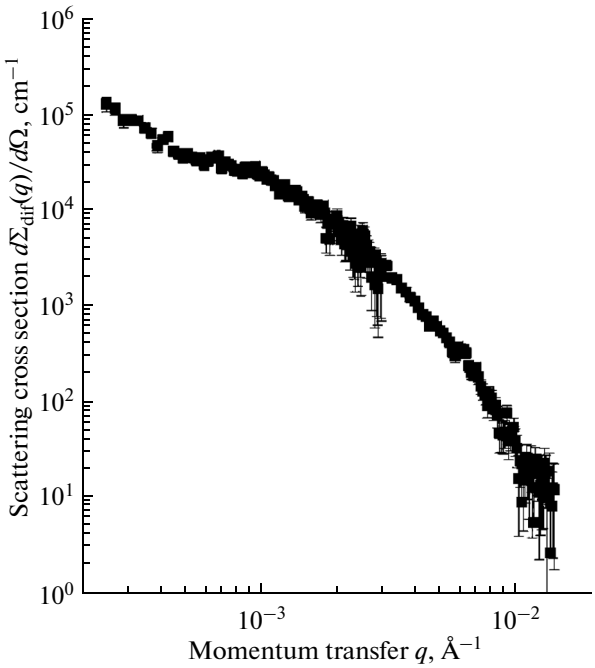

Fig. 7. Differences between the USANS cross sections for the samples coprecipitated by ammonium hydrocarbonate with and without ultrasonic treatment.

tural level (Table 2). The upper self-similarity boundary of the mass-fractal clusters can be estimated using the position of the crossover point q_c in the curve, i.e., the point of transition between the power laws q^{-n2} and q^{-n3}. In the given case, $q_c \approx 6 \times 10^{-4}$ Å^{-1}.

As it was previously noted, the scattering cross section $d\Sigma(q)/d\Omega$ of both samples obeys the power law q^{-n3} at parameters q of $3 \times 10^{-4} < q < 6 \times 10^{-4}$ Å^{-1}. The exponents $n3$ were found from the slopes of straight-line segments in the experimental curves of $d\Sigma(q)/d\Omega$. Their values are 2.3 ± 0.2 (reference sample) and 2.77 ± 0.18 (ultrasound-treated sample) (Table 2), corresponding to scattering from objects (clusters) with the mass-fractal aggregation of inhomogeneities and the fractal dimensions $D_{m3} = n3 = 2.3 \pm 0.2$ and 2.77 ± 0.18, respectively.

For both samples, the behavior of the scattering cross section $d\Sigma(q)/d\Omega$ deviates from the power law q^{-n3} at small momentum transfer $q < 3 \times 10^{-4}$ Å^{-1} . This deviation is related to the transition to the Guinier mode, where scattering depends on the characteristic size R_{c3} (i.e., the upper self-similarity boundary) of independently scattering mass-fractal aggregates.

Thus, in the case of the samples precipitated by ammonium hydrocarbonate, the overall scattering pattern evidences that they include three types of scattering inhomogeneities strongly differing in characteristic length scale. Although these structures can be independent, it is most probable that these powders comprise large-scale and rather dense mass-fractal aggregates built from mass-fractal clusters with an anisodiametrical branched structure. In turn, the latter are formed from particles that have highly developed fractal surfaces. Detailed analysis of the observed scattering pattern was performed using a generalized and unified exponential expression describing n structural levels of a scattering system [42]:

$$\frac{d\Sigma(q)}{d\Omega} = \sum_{i=1}^{m} \left(G_i \exp\left(-\frac{q^2 R_{gi}^2}{3} \right) + B_i \exp\left(-\frac{q^2 R_{g(i-1)}^2}{3} \right) \left[\frac{(\mathrm{erf}(qR_{gi}/\sqrt{6}))^3}{q} \right]^{n_i} \right). \quad (8)$$

In the above expression, summation is carried out over the number of structural levels. In the most general case, (8) includes four free parameters belonging to each structural level, such as the Guinier prefactor G_i, gyration radius R_{gi}, exponent prefactor B_i, and the power index n_i.

To obtain final results, let us reveal how expression (8) is convolved with the resolution function of the setup. The experimental dependences of the differential scattering cross section $d\Sigma(q)/d\Omega$ were processed via the LSM in the whole range under consideration. The given analysis is illustrated by data shown in Fig. 6 and presented in Table 2.

During the final stage of analysis, the influence of ultrasonic treatment on the structure of the synthe-

Table 2. Mesostructure parameters of yttrium, aluminum, and neodymium hydroxocompounds coprecipitated by ammonium hydrocarbonate with and without ultrasonic treatment. The values were obtained from USANS data

Fitting parameter	Samples	
	reference sample	ultrasound-treated sample
T_S	0.60 ± 0.01	0.56 ± 0.01
First structural level		
$G_1 \times 10^3$, cm^{-1}	5.6 ± 0.6	2.5 ± 0.5
R_{g1}, Å	360 ± 15	312 ± 10
$B_1 \times 10^{-4}$, cm^{-1} Å^{-n}	1.80 ± 0.05	3.3 ± 0.1
$D_{S1} = 6 - n1$	2.71 ± 0.03	2.82 ± 0.03
Second structural level		
$G_2 \times 10^5$, cm^{-1}	1.1 ± 0.1	2.2 ± 0.2
R_{g2}, Å	2073 ± 115	2240 ± 106
B_2, cm^{-1} Å^{-n2}	2.3 ± 0.8	2.0 ± 0.4
$D_{m2} = n2$	1.53 ± 0.05	1.59 ± 0.04
Third structural level		
$G_3 \times 10^6$, cm^{-1}	4.7 ± 0.2	4.7 ± 0.3
R_{g3}, Å	8090 ± 180	7890 ± 170
$B_3 \times 10^{-3}$, cm^{-1} Å^{-n3}	3.4 ± 1.0	0.6 ± 0.4
$D_{m3} = n3$	2.30 ± 0.20	2.77 ± 0.18

sized material was determined by comparing the properties of scattering at the reference and ultrasound-treated samples with the use of expression (7). The results of the given comparison were plotted in double logarithmic coordinates (see Fig. 7).

As in the case where the samples were precipitated by aqueous ammonia, the presented data demonstrate that the difference-curve ordinate is positive in the entire examined range of q. This shows that the reference sample makes a smaller contribution to SANS and, consequently, its nuclear density is more homogenous on the mesoscopic scale than that of the ultrasound-treated sample. This outcome agrees with the behavior of the transmission coefficient T_S of the neutron beam passed through the sample (Table 2) and its reduction is unambiguous evidence that nuclear-density fluctuations increases in the powder precipitated under ultrasonication conditions. The reasons for the given effect were discussed above.

As is obvious from analysis of the structural parameters (Table 2), ultrasonic treatment markedly affects each of the three structural levels despite the fact that the aggregation features are not significantly changed. First of all, this manifests itself in an increase in the surface fractal dimension D_{S1} and characteristic size (upper self-similarity boundary) R_{g1} of the particles of the first structural level. We note that in the precipitation of hydrated zirconium and hafnium oxides an analogous increase in the surface fractal dimension was observed in [44–46]. In addition, the degree of aggregation grows for mass-fractal clusters D_{m2} and aggregates D_{m3} of the second and third structural levels, respectively. At the same time, the characteristic sizes of the mass-fractal clusters and aggregates formed under sonocation and without it (R_{g2} and R_{g3}, respectively) do not differ from each other within the experimental errors.

It should be emphasized that, in the given case, the estimated characteristic sizes of surface-fractal particles (first structural level), mass-fractal clusters (second structural level) and fractal aggregates (third structural level) (i.e., R_{g1}, R_{g2}, and R_{g3}, respectively) are correct because the multiple scattering contribution is insignificant ($T_S > 0.5$).

CONCLUSIONS

It is demonstrated that the method for synthesizing yttrium, aluminum, and neodymium hydroxocompounds (precursors of neodymium-activated yttrium–aluminum garnet) considerably affects the features of the mesostructures of the prepared powders. In particular, almost completely nonfractal aggregates of hydroxocompounds are formed due to ammonia-assisted precipitation. At the same time, when the samples are precipitated by ammonium hydrocarbonate, three-level structure with pronounced fractal properties is formed. It is ascertained that ultrasonic treatment used during the precipitation of the aforementioned powders does not lead to a substantial change in the general structural organization of the produced materials. However, in all cases, structures with less homogeneous nuclear densities, i.e., more porous aggregates, which exhibit a more developed surface area, are generated under ultrasonication. Moreover, when hydroxocompounds are precipitated using ammonium hydrocarbonate under ultrasonication, the surface fractal dimension, as well as the degree of aggregation of the mass-fractal aggregates of particles, increases to some extent.

ACKNOWLEDGMENTS

This study was supported by the Russian Foundation for Basic Research, project no. 14-03-00907.

REFERENCES

1. J. Sanghera, B. Shaw, and W. Kim, Proc. SPIE—Int. Soc. Opt. Eng. **7912**, 79121Q-1 (2011).
2. P. P. Fedorov, in *Handbook on Solid-State Lasers: Materials, Systems and Applications*, Ed. by B. Denker and E. Shklovsky (Woodhead, Oxford, Cambridge, Philadelphia, New Delhi, 2013), p. 82.

3. M. E. Doroshenko, A. A. Demidenko, P. P. Fedorov, E. A. Garibin, P. E. Gusev, H. Jelinkova, V. A. Konyshkin, M. A. Krutov, S. V. Kuznetsov, V. V. Osiko, P. A. Popov, and J. Shulc, Phys. Status Solidi C **10**, 952 (2013).
4. A. Ikesue and K. Yoshida, J. Mater. Sci. **34**, 1189 (1999).
5. J. Lu, K. Ueda, and H. Yagi, J. Alloys Compd. **341**, 220 (2002).
6. A. A. Kaminskii, M. Sh. Akchurin, R. V. Gainutdinov, K. Takaichi, A. Shirakava, H. Yagi, T. Yanagitani, and K. Ueda, Crystallogr. Rep. **50**, 869 (2005).
7. V. B. Kravchenko and Yu. L. Kopylov, Phys. Status Solidi A **204**, 2411 (2007).
8. A. Ya. Neiman, E. V. Tkachenko, and L. A. Kvichko, Zh. Neorg. Khim. **25**, 2340 (1980).
9. V. B. Glushkova, O. N. Egorova, and V. A. Krzhizhanovskaya, Izv. Akad. Nauk SSSR, Neorg. Mater. **19**, 95 (1983).
10. X. Y. Chen, L. Yang, and R. E. Cook, Nanotecnology **14**, 670 (2003).
11. J. G. Li, T. Ikegami, and J. H. Lee, J. Eur. Ceram. Soc. **20**, 2395 (2000).
12. E. Caponetti, S. Enzo, and B. Lasio, Opt. Mater. **29**, 1240 (2007).
13. T. Chudoba, M. Teyssier, and W. Lojkowski, Solid State Phenom. **128**, 41 (2007).
14. J. G. Li, T. Ikegami, and J. H. Lee, J. Mater. Res. **15**, 2375 (2000).
15. C.-C. Chiang, M.-S. Tsai, and M.-H. Hon, J. Electrochem. Soc. **154**, 326 (2007).
16. V. A. Maslov, V. V. Voronov, R. P. Ermakov, V. V. Shcherbakov, V. A. Usachev, N. E. Kononenko, and P. P. Fedorov, Vestn. MGTU, Ser. Priborostroen., Spets. Vyp. Radioopt. Tekhnol. Priborostroen., 20 (2012).
17. P. E. Meskin, A. E. Baranchikov, V. K. Ivanov, E. V. Kisterev, A. A. Burukhin, B. R. Churagulov, N. N. Oleinikov, Sh. Komarneni, and Yu. D. Tretyakov, Dokl. Chem. **389**, 62 (2003).
18. P. E. Meskin, F. Yu. Sharikov, V. K. Ivanov, B. R. Churagulov, and Yu. D. Tretyakov, Mater. Chem. Phys. **104**, 439 (2007).
19. P. E. Meskin, A. E. Baranchikov, V. K. Ivanov, D. R. Afanas'ev, A. I. Gavrilov, B. R. Churagulov, and N. N. Oleinikov, Inorg. Mater. **40**, 1058 (2004).
20. P. E. Meskin, A. I. Gavrilov, V. D. Maksimov, V. K. Ivanov, and B. R. Churagulov, Russ. J. Inorg. Chem. **52**, 1648 (2007).
21. A. Ye. Baranchikov, V. K. Ivanov, and Yu. D. Tretyakov, Ultrason. Sonochem. **14**, 131 (2007).
22. A. E. Baranchikov, V. K. Ivanov, N. N. Oleinikov, and Yu. D. Tretyakov, Inorg. Mater. **40**, 1091 (2004).
23. A. E. Baranchikov, V. K. Ivanov, A. N. Baranov, N. N. Oleinikov, and Yu. D. Tretyakov, Russ. J. Inorg. Chem. **46**, 1874 (2001).
24. A. Radulescu, E. Kentzinger, J. Stellbrink, et al., Neutron News **16**, 7 (2005).
25. G. Goerigk and Z. Varga, J. Appl. Crystallogr. **44**, 337 (2011).
26. G. D. Wignall and F. S. Bates, J. Appl. Crystallogr. **20**, 28 (1987).
27. www.iff.kfa-juelich.de/~pipich/doku-wiki/doku.php/qtikws
28. W. Schmatz, T. Springer, J. Schelten, and K. Ibel, J. Appl. Crystallogr. **7**, 96 (1974).
29. C. E. Holcombe, J. Am. Ceram. Soc. **61**, 481 (1978).
30. M. D. Rasmussen, M. Akinc, and O. Hunter, Ceram. Int. **11**, 51 (1985).
31. E. A. Frolova, D. F. Kondakov, A. D. Yapryntsev, A. E. Baranchikov, V. K. Ivanov, and V. P. Danilov, Russ. J. Inorg. Chem. **60**, 259 (2015).
32. A. D. Yapryntsev, A. E. Baranchikov, A. V. Zabolotskaya, L. P. Borilo, and V. K. Ivanov, Russ. J. Inorg. Chem. **59**, 1383 (2014).
33. A. D. Yaprynsev, A. E. Baranchikov, L. S. Skogareva, A. E. Goldt, I. P. Stolyarov, O. S. Ivanova, V. V. Kozik, and V. K. Ivanov, CrystEngComm **17**, 2667 (2015).
34. A. E. Baranchikov, A. D. Yapryntsev, A. E. Goldt, and V. K. Ivanov, Curr. Microwave Chem. 3, 3 (2015).
35. V. Petříček, M. Dušek, and L. Palatinus, Z. Kristallogr. **229**, 345 (2014).
36. R. D. Shannon, Acta Crystallogr. A **32**, 751 (1976).
37. A. D. Yapryntsev, A. E. Baranchikov, N. N. Gubanova, V. K. Ivanov, and Yu. D. Tretyakov, Inorg. Mater. **48**, 494 (2012).
38. K. Hayashi, S. Toyoda, H. Takebe, and K. Morinaga, J. Ceram. Soc. Jpn. **99**, 550 (1991).
39. E. L. Head and C. E. Holly, *Rare Earth Research*, Ed. by L. Eyring (Gordon and Breach, New York, 1965), Vol. 3, p. 707.
40. H. D. Bale and P. W. Schmidt, Phys. Rev. Lett. **38**, 596 (1984).
41. A. Guinier, G. Fournet, C. B. Walker, and K. L. Yudowitch, *Small Angle Scattering of X-Rays* (Wiley, New York, 1955), p. 17.
42. G. Beaucage, J. Appl. Crystallogr. **28**, 717 (1995).
43. S. V. Maleyev, Phys. Rev. B **52**, 13163 (1995).
44. V. K. Ivanov, G. P. Kopitsa, A. Ye. Baranchikov, M. Sharp, K. Pranzas, and S. V. Grigoriev, Russ. J. Inorg. Chem. **54**, 2091 (2009).
45. G. P. Kopitsa, A. E. Baranchikov, O. S. Ivanova, A. D. Yapryntsev, S. V. Grigoriev, P. K. Pranzas, and V. K. Ivanov, J. Phys.: Conf. Ser. **340**, 012057 (2012).
46. N. N. Gubanova, A. Ye. Baranchikov, G. P. Kopitsa, L. Almásy, B. Angelov, A. D. Yapryntsev, L. Rosta, andb V. K. Ivanov, Ultrason. Sonochem. **24**, 230 (2015).

Translated by S. Rodikov